

# Core Formation in Dwarf Halos with Self Interacting Dark Matter: No Fine-Tuning Necessary

Oliver D. Elbert<sup>1\*</sup>, James S. Bullock<sup>1</sup>, Shea Garrison-Kimmel<sup>1</sup>, Miguel Rocha<sup>2</sup>,

Jose Oñorbe<sup>1,3</sup>, Annika H. G. Peter<sup>4</sup>

<sup>1</sup>Center for Cosmology, Department of Physics and Astronomy, University of California, Irvine, CA 92697, USA

<sup>2</sup>SciTech Analytics, Inc., Santa Cruz, CA, 95062, USA

<sup>3</sup>Max Planck Institut fuer Astronomie, Koeningstuhl 17, 69117 Heidelberg, Germany

<sup>4</sup>CCAPP, Department of Physics, and Department of Astronomy, The Ohio State University, Columbus, OH, 43210, USA

5 December 2014

## ABSTRACT

We investigate the effect of self-interacting dark matter (SIDM) on the density profiles of  $V_{\max} \simeq 40 \text{ km s}^{-1}$  isolated dwarf dark matter halos – the scale of relevance for the too big to fail problem (TBTF) – using very high-resolution cosmological zoom simulations. Each halo has millions of particles within its virial radius. We find that SIDM models with cross sections per unit mass spanning the range  $\sigma/m = 0.5 - 50 \text{ cm}^2 \text{ g}^{-1}$  alleviate TBTF and produce constant density cores of size  $300 - 1000 \text{ pc}$ , comparable to the half-light radii of  $M_* \sim 10^{5-7} M_{\odot}$  dwarfs. The largest, lowest density cores develop for cross sections in the middle of this range,  $\sigma/m \sim 5 - 10 \text{ cm}^2 \text{ g}^{-1}$ . Our largest SIDM cross section run ( $\sigma/m = 50 \text{ cm}^2 \text{ g}^{-1}$ ) develops a slightly denser core owing to mild core-collapse behavior, but it remains less dense than the CDM case and retains a constant density core profile. Our work suggests that SIDM cross sections as large or larger than  $50 \text{ cm}^2 \text{ g}^{-1}$  remain viable on velocity scales of dwarf galaxies ( $v_{\text{rms}} \sim 40 \text{ km s}^{-1}$ ). The range of SIDM cross sections that alleviate TBTF and the cusp/core problem spans at least two orders of magnitude and therefore need not be particularly fine-tuned.

**Key words:** dark matter – cosmology: theory – galaxies: haloes

## 1 INTRODUCTION

Cosmological studies of the large-scale universe have provided tremendous evidence in favor of a Universe dominated by dark matter (DM) and dark energy (e.g. Komatsu et al., 2011; Hinshaw et al., 2013; Planck Collaboration et al., 2014), but thus far very little is known about the underlying nature of the DM particle other than that it is long-lived and that it interacts weakly with the standard model. For thermal particles, the dark matter needs to be fairly massive (or “cold” – non-relativistic at decoupling) in order to produce a power spectrum consistent with large-scale structure (Reid et al., 2010). Weakly interacting massive particles (WIMPs), for example, provide a compelling and well-motivated class of CDM candidates (Steigman & Turner, 1985; Griest, 1988; Jungman et al., 1996). On the scales of concern for galaxy formation, WIMPs behave as collisionless particles and are one of the prime motivations for what has become the standard paradigm for structure formation: collisionless Cold Dark Matter (CDM).

There are, however, disagreements between predictions from

CDM-only simulations and observations on small scales. For example, some galaxies appear to have flat central density profiles (e.g. Flores & Primack, 1994; Kuzio de Naray et al., 2008; Amorisco et al., 2014; Oh et al., 2008; Walker & Peñarrubia, 2011, but also see Strigari et al., 2014) with core-like log-slopes ( $\alpha \sim 0$ ) rather than the predicted cusps ( $\alpha \sim 1$ ) seen in CDM simulations (Dubinski & Carlberg, 1991; Navarro et al., 1997). This issue is known as the cusp/core problem. A qualitatively similar anomaly was pointed out by Boylan-Kolchin et al. (2011, 2012), who showed that observations of the dwarf spheroidal (dSph) satellites of the Milky Way (MW) imply central masses well below those of the  $V_{\max} = 40 \text{ km s}^{-1}$  halos that appear to be common in ultra-high resolution simulations of MW-size hosts (e.g. Diemand et al., 2008; Springel et al., 2008). This issue is known as the “too big to fail” problem (TBTF). Tollerud et al. (2014) and Garrison-Kimmel et al. (2014b) further showed that the Andromeda (M31) dSph satellites and the field galaxies near the MW and M31, respectively, suffer from the same problem. Studies of larger samples of dwarf galaxies in the field also indicate a similar density problem at a comparable velocity scale  $V_{\max} \simeq 40 \text{ km s}^{-1}$  (Ferrero et al., 2012; Klypin et al., 2014; Papastergis et al., 2014).

One natural solution to the TBTF problem and other central-

\* oelbert@uci.edu

density issues is to posit that galaxy halos have lower core densities than predicted in CDM-only simulations. For example, baryonic processes may act to reduce and flatten the central densities of small galaxies in CDM (e.g. Pontzen & Governato, 2012; Governato et al., 2012; Di Cintio et al., 2014; Navarro et al., 1996). In contrast, Peñarrubia et al. (2012) and Garrison-Kimmel et al. (2013) have argued that the  $M_* \sim 10^6 M_\odot$  galaxies of interest for TBTF have not had enough supernovae to alter densities sufficiently (though see Amorisco et al., 2014; Gritschneider & Lin, 2013). Others have suggested environmental effects may increase the efficacy of these internal processes by similarly reducing the central masses of subhalos (e.g. Zolotov et al., 2012; Del Popolo, 2012; Arraki et al., 2014; Brooks & Zolotov, 2014; Del Popolo et al., 2014). However, these external processes are weak or non-existent in the field, suggesting that non-baryonic solutions may be necessary to solve the discrepancy observed outside the MW and M31 (Garrison-Kimmel et al., 2014b; Papastergis et al., 2014). Similarly, while large TBTF subhalos become increasingly infrequent as the mass of the MW and M31 host halos decrease (Purcell & Zentner, 2012; Wang et al., 2012; Rodríguez-Puebla et al., 2013; Cautun et al., 2014), solutions of this kind appear less likely in the face of evidence that the TBTF problem is persistent in the field (Ferrero et al., 2012; Klypin et al., 2014; Garrison-Kimmel et al., 2014b).

Alternatively, the central density issues may be telling us something about cosmology. For example, if the primordial power spectrum is non-standard (Zentner & Bullock, 2002; Polisensky & Ricotti, 2014; Garrison-Kimmel et al., 2014c) or the dark matter is warm rather than cold (Anderhalden et al., 2013; Lovell et al., 2014; Horiuchi et al., 2014) then the central densities of dark matter halos would decrease. However, neither of these possibilities produce constant-density cores on observable scales; they simply lower the normalization while retaining cuspy slopes.

The focus of this paper is to explore an alternative possibility: that the CDM particles are strongly self-interacting.<sup>1</sup> First discussed in an astrophysical context by Spergel & Steinhardt (2000), Self-Interacting Dark Matter (SIDM) with energy-exchange cross sections per unit mass of order  $\sigma/m \sim 1 \text{ cm}^2 \text{ g}^{-1}$  can naturally produce constant-density cores in the hearts of dark matter halos on the scales of relevance for galaxy rotation curves and the TBTF problem (Burkert, 2000; Davé et al., 2001; Vogelsberger et al., 2012; Rocha et al., 2013). Constant density isothermal cores in SIDM halos come about because kinetic energy can be transmitted from the hot outer halo inward (see, e.g., the discussion in Rocha et al., 2013). This effect can only occur if  $\sigma/m$  is large enough for there to be a relatively high probability of scattering over a time  $t_{\text{age}}$  comparable to the age of the halo:  $\Gamma \times t_{\text{age}} \sim 1$ , where  $\Gamma \simeq \rho_{\text{dm}}(\sigma/m)v_{\text{rms}}$  is the interaction rate,  $\rho_{\text{dm}}$  is the local dark matter density, and  $v_{\text{rms}}$  is the rms speed of dark-matter particles. If the cross section is too large, however, then the high probability of interaction can potentially lead to a negative heat flux, where energy is transmitted from the inside out (Kochanek & White, 2000), leading to a “core collapse” phenomena, not unlike core collapse in globular clusters, where the central halo density increases to the point that it exacerbates the over-density problem on small scales. The specific range of cross sections that are a) small enough to be observationally allowed, b) large enough to alleviate the relevant

small-scale problems, and c) small enough to avoid catastrophic core collapse, are all topics of this exploration.

In most particle-physics based models for SIDM, the scattering interactions have a velocity dependence (e.g., Loeb & Weiner, 2011; Tulin et al., 2013a; Kaplinghat et al., 2014; Boddy et al., 2014b,a). Astrophysical constraints, on the other hand, tend to rely on specific classes of objects that have a characteristic  $v_{\text{rms}}$  scale, meaning that they constrain  $\sigma(v)/m$  at a specific value of  $v \simeq v_{\text{rms}}$ . The best published limits ( $\sigma/m \lesssim 1 \text{ cm}^2 \text{ g}^{-1}$ ) come from galaxy clusters with characteristic rms velocities  $v_{\text{rms}} \simeq 1000 \text{ km s}^{-1}$  (Yoshida et al., 2000; Gnedin & Ostriker, 2001; Randall et al., 2008; Rocha et al., 2013; Peter et al., 2013). At the same time, the most compelling astrophysical *motivations* for exploring SIDM in the first place occur on the scales of dwarf galaxies where  $v_{\text{rms}} \simeq 10 - 100 \text{ km s}^{-1}$ . These differences in velocity scale are significant. For example, the SIDM cross section could vary as  $\sigma/m \propto v^{-4}$  if the interaction were a dark version of Rutherford scattering, with a massless force carrier (Tulin et al., 2013b). Thus it is not outlandish to consider the possibility that DM self-interactions on the scale of dwarf galaxies are *four orders of magnitude larger* than they are on the scale of galaxy clusters. Clearly we have significant need to derive constraints on as many velocity scales as possible.

The potential for significant velocity scaling in the SIDM energy-exchange cross section has motivated Vogelsberger et al. (2012) and Zavala et al. (2013) to explicitly run zoom simulations of Milky Way-size hosts using SIDM with velocity-dependent  $\sigma/m$  values tuned to evade bounds on cluster scales and to have large values ( $\sim 10 \text{ cm}^2 \text{ g}^{-1}$ ) on the scale of problematic TBTF halos ( $v_{\text{rms}} \simeq V_{\text{max}} \simeq 40 \text{ km s}^{-1}$ ). They show that the TBTF problem is resolved for  $\sigma/m \simeq 1 - 10 \text{ cm}^2 \text{ g}^{-1}$  on the velocity scale of dwarfs. We note that Figure 8 of Vogelsberger et al. (2012) makes clear that a run with  $\sigma/m = 10 \text{ cm}^2 \text{ g}^{-1}$  provides a particularly good match to the spread in dwarf satellite central densities seen around the Milky Way.

The goal of this paper is to explore more fully a range of cross sections at the dwarf scales of interest, focusing specifically on isolated halos rather than subhalos in order to achieve very high resolution. We run a set of ultra-high resolution cosmological simulations of isolated dwarf halos with  $v_{\text{rms}} \simeq 40 \text{ km s}^{-1}$  using SIDM cross sections  $\sigma/m = 0.1 - 50 \text{ cm}^2 \text{ g}^{-1}$  in addition to collisionless CDM. The aim is to quantify the range of cross sections that can alleviate the TBTF problem (in the field) and are expected to produce observable cores in small dwarf galaxies. We also investigate whether a certain range of cross sections can be ruled out because they would result in catastrophic core collapse.

This work is organized as followed. In §2, we describe the simulations and analysis pipeline. We present our results in §3, focusing first on the impact of varying  $\sigma/m$  on the density profiles in §3.1 and then on the implications for TBTF in §3.2. We summarize our results and conclude in §4.

## 2 SIMULATIONS

As we demonstrate explicitly below, in order to resolve the relevant  $\sim 300 - 1000 \text{ pc}$  scales of classical dwarf spheroidal galaxies, very high force and mass resolution are required. We achieve this resolution in cosmological simulations using the zoom technique (Katz & White, 1993; Oñorbe et al., 2014). Our SIDM implementation follows that described in Rocha et al. (2013), using a modified version of GADGET-2 (Springel, 2005). Halos were identified with

<sup>1</sup> SIDM models with primordial power spectra that deviate from CDM on small scales have been explored by Buckley et al. (2014) but we focus on CDM-type power spectra here.

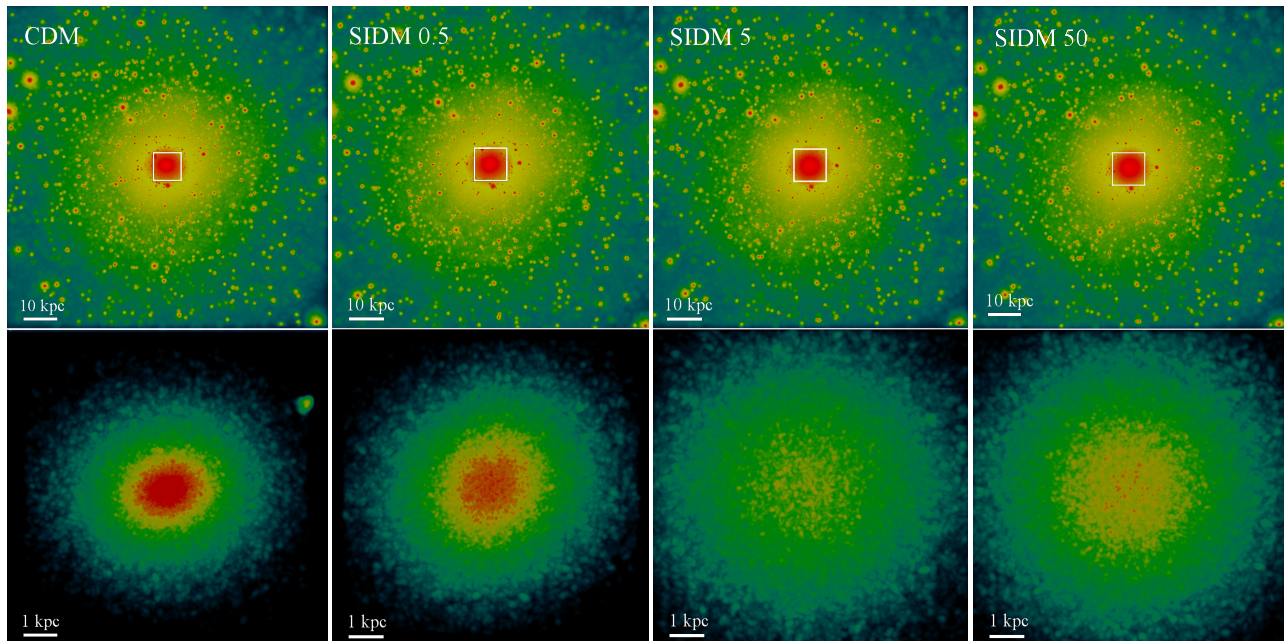


**Figure 1.** Dark matter density of Pippin in CDM (left) and SIDM with  $\sigma/m$  increasing from left to right: 0.5, 5, and 50  $\text{cm}^2 \text{g}^{-1}$ . Boxes on the top span 100 kpc ( $R_v = 55 \text{kpc}$ ) and the bottom panel zooms in to span a central 10 kpc box (with modified color bar). Notice that the global properties of the halos on the scale of the virial radius, including the number and locations of subhalos, are nearly identical across all runs. The only difference is that the inner core regions become less dense and somewhat puffed out in the SIDM cases. Note that the 50  $\text{cm}^2 \text{g}^{-1}$  simulation is somewhat denser in the inner core than the 5  $\text{cm}^2 \text{g}^{-1}$  case; it is undergoing mild core collapse.

Name	$M_v$ ( $10^{10} M_\odot$ )	$R_v$ (kpc)	$V_{\text{max}}$ ( $\text{km s}^{-1}$ )	$N_p(R_v)$ ( $10^6$ )	$\sigma/m$ ( $\text{cm}^2 \text{g}^{-1}$ )
Pippin	0.9	55	37	4.1	0, 0.1, 0.5, 5, 10, 50
Merry	1.2	59	38	5.4	0, 0.5, 1, 10

**Table 1.** Summary of simulated halos. The first four columns list identifying names and virial-scale properties (virial mass, virial radius, and maximum circular velocity). The fifth column gives number of particles within the virial radius for the high-resolution runs and the last column summarizes the cross sections each halo was simulated with. The virial-scale properties of the halos listed are for the CDM cases ( $\sigma/m = 0$ ) but each of these values remains unchanged (within  $\sim 5\%$ ) for all SIDM runs.  $M_v$  and  $R_v$  are calculated using the Bryan & Norman (1998) definition of  $\rho_v$ .

the six-dimensional phase-space halo finder ROCKSTAR (Behroozi et al., 2013).

We chose two halos for our primary simulations using parent cosmological volumes of 7 Mpc on a side. Initial conditions were generated with MUSIC (Hahn & Abel, 2011) at  $z = 125$  using cosmological parameters derived from the *Wilkinson Microwave Anisotropy Probe-7* year data (Komatsu et al., 2011):  $h = 0.71$ ,  $\Omega_m = 0.266$ ,  $\Omega_\Lambda = 0.734$ ,  $n_s = 0.963$ , and  $\sigma_8 = 0.801$ . Their global properties are given in Table 1. We refer to the slightly smaller of the two dwarfs ( $V_{\text{max}} = 37 \text{ km s}^{-1}$ ) as Pippin and the larger ( $V_{\text{max}} = 38 \text{ km s}^{-1}$ ) as Merry. Our high resolution runs, which we analyze throughout, have particle mass  $m_p = 1.5 \times 10^3 M_\odot$  and a Plummer equivalent force softening  $\epsilon = 28 \text{ pc}$ . We have also checked that various basic parameters of our target halos (spins, concentrations and formation times) are within one standard deviation of what is expected for dwarf halos

based on a larger simulation box of 35 Mpc on a side (described in Oñorbe et al., 2014).

In addition to  $\sigma/m = 0$  (collisionless CDM) runs, we simulate both halos with  $\sigma/m = 0.5, 1, 10 \text{ cm}^2 \text{g}^{-1}$ . Additionally we have simulated Pippin with  $\sigma/m = 0.1, 5, 50 \text{ cm}^2 \text{g}^{-1}$ . In all SIDM simulations, the dark matter self-interactions were calculated using an SIDM smoothing length equal to  $0.25\epsilon$ , as described in Rocha et al. (2013).

Figure 1 shows visualizations of Pippin at high resolution, colored by the local dark matter density, with collisionless CDM on the far left and SIDM runs of increasing cross section to the right. The upper panels visualize a box 100 kpc across ( $\sim 2R_v$ ) and the lower panels zoom in on the central 10 kpc of the halos, using a color bar that has been rescaled to emphasize the highest densities. As these visualizations emphasize, bulk halo properties on the scale of  $R_v$  are virtually identical in CDM and SIDM; even the locations of subhalos remain unchanged. The fact that substructure remains very similar in both SIDM and CDM is consistent with the findings of Vogelsberger & Zavala (2013) and Rocha et al. (2013); here, however, we examine mass scales well below those resolved in any previous SIDM study, resolving substructure as small as  $V_{\text{max}} = 1 \text{ km s}^{-1}$ . The main differences are apparent in the core regions (lower panels), where the SIDM runs are systematically less dense than CDM. Note that the 50  $\text{cm}^2 \text{g}^{-1}$  run is actually denser in its core than the 5  $\text{cm}^2 \text{g}^{-1}$  run. As discussed below, this is a result of core collapse.

## 2.1 Resolution Tests

We have designed our high-resolution simulations explicitly to recover the density structure at the  $\sim 300 \text{ pc}$  half-light radius scale of low-mass dwarfs based on the work of Power et al. (2003) for CDM simulations. Power et al. (2003) showed that the differential

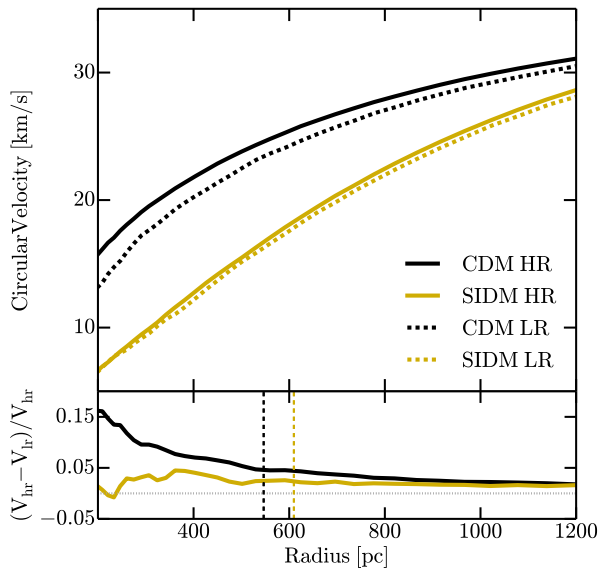


**Figure 2.** *Top:* Circular velocity profiles of Pippin at our fiducial resolution (solid;  $m_p = 1.5 \times 10^3 M_\odot$ ,  $\epsilon = 28$  pc) and at low resolution (dotted;  $m_p = 1.2 \times 10^4 M_\odot$ ,  $\epsilon = 84$  pc) for both CDM (black) and SIDM ( $1 \text{ cm}^2 \text{ g}^{-1}$ , yellow). *Bottom:* The relative difference between high and low resolution circular velocity profiles. The dashed vertical lines indicate the Power et al. (2003) radius for the low resolution halos. Note that the SIDM halos are much better converged than the CDM simulations.

density profiles of CDM halos should be converged only outside of a specific radius where the gravitational two-body relaxation time approximates the Hubble time. While this work is perfectly well-designed for CDM runs, the issue of convergence in SIDM is less well explored. In order to remedy this concern, we have simulated Pippin in CDM and SIDM ( $1 \text{ cm}^2 \text{ g}^{-1}$ ) at lower resolution, with eight times worse mass resolution ( $m_p = 1.2 \times 10^4 M_\odot$ ) and with greater force softening ( $\epsilon = 84$  pc) than our high resolution runs. As expected, we confirm that the differential density profile of the CDM halo is convergent down to the classic Power et al. (2003) radius of the low resolution runs (168 pc for Pippin, 160 pc for Merry); reassuringly, the SIDM run is even more stable. We find convergence in the density profile down to below half the Power radius (see also Vogelsberger et al., 2012, who found similar robustness for SIDM halos). This is qualitatively reasonable in the limit where physical self-interactions are more important than artificial two-body interactions.

While the differential density is the most natural theoretical quantity to consider in a convergence study, observationally the circular velocity (or cumulative mass) is more relevant. Velocity curves suffer more from numerical convergence issues because they rely on the integrated density. Figure 2 shows the circular velocity profiles of the low (dashed) and high resolution (solid) simulations with CDM in black and SIDM in yellow. The lower panel shows the relative difference as a function of radius, with the Power radii of the low resolution runs marked for comparison as vertical dashed lines. The low resolution rotation curve in CDM starts to under-predict visibly compared to the higher resolution run at about 1.4 times the Power radius (some 14 times the formal force softening  $\epsilon$ ) and disagrees by more than 5% at  $\sim 1.2 \times r_{\text{Power}}$ . The SIDM run, however, remains reasonably well converged throughout: the

high and low resolution simulations do not disagree by more than 4% outside of  $\sim 0.6 \times r_{\text{Power}}$ , and not by more than 5% outside of 100 pc.

For the remainder of this work, we present high resolution density profiles of CDM halos down to the Power radius and to half the Power radius for SIDM profiles. Based on the work presented in this section, we believe that the full regions plotted are converged. For rotation curves, we plot both CDM and SIDM halos to 200 pc. This is the  $1.2r_{\text{Power}}$  limit for the CDM curves, where we expect them to be correct within  $\lesssim 5\%$ . The SIDM rotation curves are accurate to the last plotted point.

### 3 RESULTS

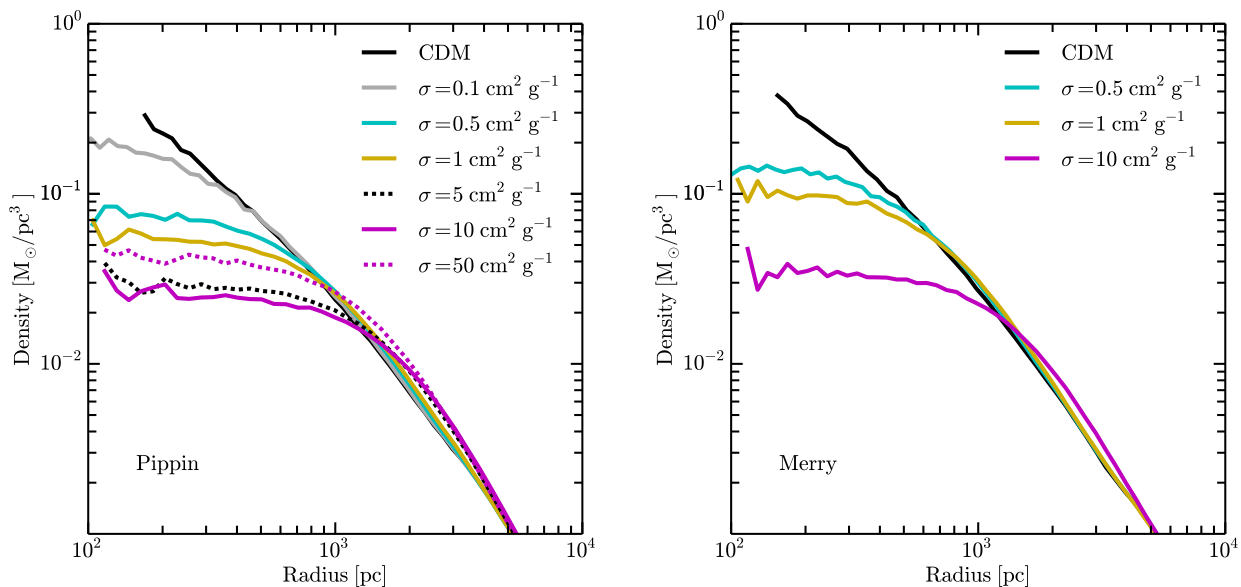
#### 3.1 Halo Profiles

Figure 3 presents the density profiles of our resultant halos. While the  $\sigma/m = 0.1 \text{ cm}^2 \text{ g}^{-1}$  run of Pippin produces only a modest reduction in core density compared to CDM, all SIDM runs with  $\sigma/m \geq 0.5 \text{ cm}^2 \text{ g}^{-1}$  result in substantial  $\sim 500 - 1000$  pc cores, with reduced central densities compared to CDM. As the SIDM cross section is increased from  $\sigma/m = 0.1 \rightarrow 5 - 10 \text{ cm}^2 \text{ g}^{-1}$  the cores become increasingly extended and have lower central densities. However, the Pippin run with  $\sigma/m = 50 \text{ cm}^2 \text{ g}^{-1}$  has a denser core than the  $\sigma/m = 10 \text{ cm}^2 \text{ g}^{-1}$  case. This is almost certainly due to core-collapse behavior (e.g. Kochanek & White, 2000; Balberg et al., 2002; Colín et al., 2002; Koda & Shapiro, 2011). As illustrated and discussed in Appendix A, the velocity dispersion profile of this run is noticeably hotter in the core than in the outer regions – a clear indication that a negative heat flux is in action. However, note that even a cross-section as large as  $50 \text{ cm}^2 \text{ g}^{-1}$  results in a significantly lower central density than the CDM case, with a clear constant-density core within  $\sim 500$  pc. Evidently, for this particular halo at least, a cross section as large as  $50 \text{ cm}^2 \text{ g}^{-1}$  does not produce run-away core collapse, but rather a mild increase in the central density compared to a run with ten times weaker self-interaction ( $5 \text{ cm}^2 \text{ g}^{-1}$ ).

Our results on core collapse are not significantly different than those reported most recently in the literature. Older simulations of isolated halos showed core recollapse after a few dynamical times for an equivalent cross section larger than  $\sim 5 \text{ cm}^2 \text{ g}^{-1}$  (scaled appropriately to the mass of Pippin; Kochanek & White, 2000; Balberg et al., 2002; Koda & Shapiro, 2011). However, cosmological halos only see core collapse for higher cross sections, and not consistently for a fixed halo mass (Yoshida et al., 2000; Colín et al., 2002; Davé et al., 2001; Rocha et al., 2013). The primary reason for this difference is that accretion of new matter onto the halo stabilizes the heat flow within the halo (Yoshida et al., 2000; Colín et al., 2002). Vogelsberger et al. (2012) saw evidence for core collapse only for their largest constant cross section run ( $\sigma/m = 10 \text{ cm}^2 \text{ g}^{-1}$ ) and, even then, only for one subhalo (out of the  $\sim 10$  most massive they studied). This is broadly consistent with the behavior we see.

#### 3.2 Circular Velocities and the Too Big to Fail problem

According to the ELVIS simulations of the Local Group (Garrison-Kimmel et al., 2014a), there should be  $\sim 10$  isolated halos with  $V_{\text{max}} \gtrsim 40 \text{ km s}^{-1}$  in the local ( $\sim 1.2$  Mpc) field around the MW and M31, excluding satellites of either large system. Of the fourteen isolated dwarfs in this volume, only one (Tucana) is clearly



**Figure 3.** Density profiles of Pippin (left) and Merry (right) in collisionless CDM and in SIDM (see legend) at  $z = 0$ . All SIDM runs with  $\sigma/m \geq 0.5 \text{ cm}^2 \text{ g}^{-1}$  produce central density profiles with well-resolved cores within  $\sim 500$  pc. Core densities are the lowest (and core sizes the largest) for cross sections in the range  $\sigma/m = 5 - 10 \text{ cm}^2 \text{ g}^{-1}$ . The  $50 \text{ cm}^2 \text{ g}^{-1}$  run of Pippin has undergone a mild core collapse, with a resultant central density intermediate between the  $10 \text{ cm}^2 \text{ g}^{-1}$  run and  $1 \text{ cm}^2 \text{ g}^{-1}$  run. For velocity dispersion profiles of these halos, see Appendix A. NFW fits to the CDM profiles of each halo yield scale radii of  $\sim 2.7$  kpc.

dense enough to reside in a CDM halo larger than  $40 \text{ km s}^{-1}$ . The rest appear to reside in halos that are significantly less dense than expected for the ten most massive systems predicted in CDM simulations. These missing, or overdense,  $V_{\text{max}} \simeq 40 \text{ km s}^{-1}$  halos are the systems of concern for the TBTF problem.

Figure 4 illustrates this problem explicitly by comparing the circular velocities of nearby field dwarfs at their half-light radius (data points) to the circular velocity profiles of our simulated halos (lines), each of which has  $V_{\text{max}} \simeq 40 \text{ km s}^{-1}$  and is therefore nominally a TBTF halo. The data points indicate dwarf galaxies ( $M_* < 1.7 \times 10^7$ ) farther than 300 kpc from both the Milky Way and Andromeda that are dark matter dominated within their half-light radii ( $r_{1/2}$ ), with estimates for their circular velocities at  $r_{1/2}$  ( $V_{1/2}$ ). We have excluded Tucana, which has an implied central density so high that it is hard to understand even in the context of CDM (see Garrison-Kimmel et al., 2014b, for a discussion).  $V_{1/2}$  for the purely dispersion galaxies are calculated using the Wolf et al. (2010) formula, where measurements for stellar velocity dispersion,  $\sigma_*$ , are taken from Hoffman et al. (1996), Simon & Geha (2007), Epinat et al. (2008), Fraternali et al. (2009), Collins et al. (2013), and Kirby et al. (2014). However, WLM and Pegasus also display evidence of rotational support, indicating that they are poorly described by the Wolf et al. (2010) formalism. For the former, we use the Leaman et al. (2012) estimate of the mass within the half-light radius, obtained via a detailed dynamical model. The data point for Pegasus is obtained via the method suggested by Weiner et al. (2006), wherein  $\sigma_*^2$  is replaced with  $\sigma_*^2 + \frac{1}{2}(v \sin i)^2$  in the Wolf et al. (2010) formula, where  $v \sin i$  is the projected rotation velocity (also see §5.2 of Kirby et al., 2014).

As expected, the data points all lie below the CDM curves (black lines), demonstrating explicitly that both Merry and Pippin are TBTF halos. The SIDM runs, however, provide a much better

match, and in fact all of the SIDM runs with  $\sigma/m \geq 0.5 \text{ cm}^2 \text{ g}^{-1}$  alleviate TBTF.

### 3.3 Expectations for the stellar-mass halo-mass relation

A problem related to TBTF, but in principle distinct from it, concerns the relationship between the observed core densities of galaxies and their stellar masses. Specifically, there does not appear to be any correlation between stellar mass and inner dark matter density inferred from dynamical estimates of dwarf galaxies in the Local Group (Strigari et al., 2008; Boylan-Kolchin et al., 2012; Garrison-Kimmel et al., 2014b). If dark matter halos behave as expected in dissipationless  $\Lambda$ CDM simulations, then we would expect more massive galaxies to have higher dark matter densities at fixed radius. This ultimately stems from the expectation, borne out at higher halo masses, that more massive dark matter halos tend to host more massive galaxies.

Consider, for example, the two galaxies Pegasus ( $r_{1/2} \simeq 1$  kpc) and Leo A ( $r_{1/2} \simeq 500$  pc) in Figure 4. Both of these galaxies have about the same stellar mass  $M_* \simeq 10^7 M_\odot$ . According to the expectations of abundance matching (Garrison-Kimmel et al., 2014b), each of these galaxies should reside within a  $V_{\text{max}} \simeq 40 \text{ km s}^{-1}$  halo. Instead, their central densities are such that, if their dark matter structure follows the CDM-inspired NFW form, they need to have drastically different potential well depths:  $V_{\text{max}} \simeq 30$  and  $12 \text{ km s}^{-1}$  for Pegasus and Leo A, respectively (see Figure 12 of Garrison-Kimmel et al., 2014b). However, if we instead interpret their densities in the context of SIDM, the results are much more in line with abundance matching expectations.

Abundance matching relations remain unchanged in SIDM because halo mass functions in SIDM are identical to those in CDM (Rocha et al., 2013). That is, in SIDM, just like CDM, we would naively expect both Pegasus and Leo A to reside in ha-

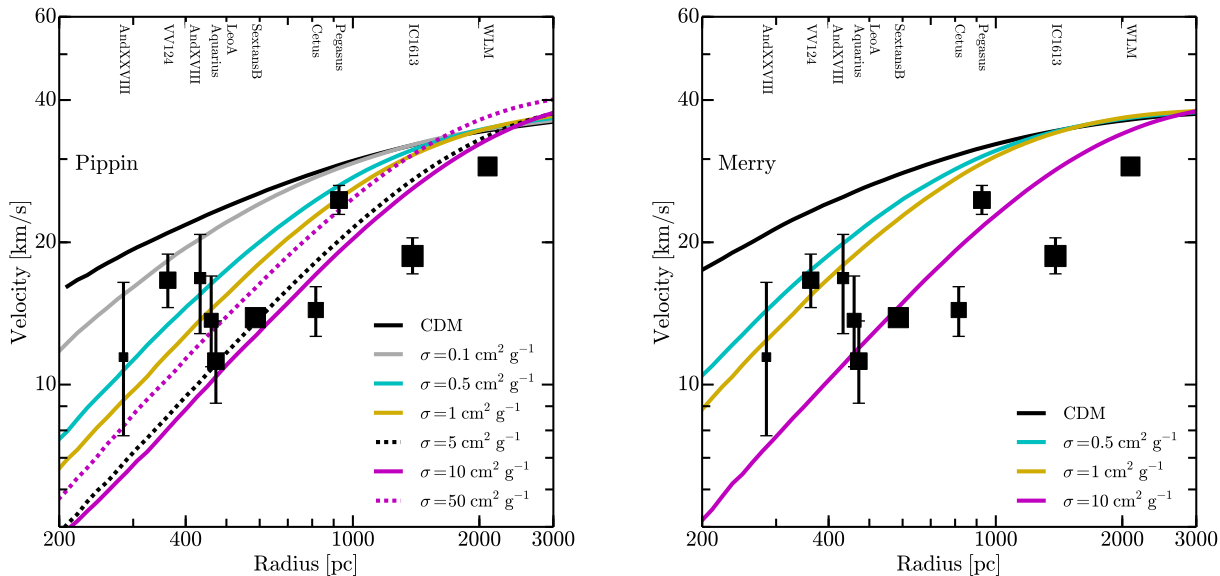


**Figure 4.** Circular velocity profiles of Pippin (left) and Merry (right) simulated with CDM (solid black) and various SIDM cross-sections (see legend). Halos of this mass ( $V_{\max} \simeq 40 \text{ km s}^{-1}$ ) should be fairly common within the  $\sim 1 \text{ Mpc}$  Local Field of the Milky Way. The data points indicate measurements of the circular velocity at the half-light radii of Local Field (as defined in Garrison-Kimmel et al., 2014b) dwarf galaxies (see references in text). The sizes of the points scale with the stellar mass of the galaxy, with the smallest AndXXVIII at  $M_{\star} \simeq 3 \times 10^5 M_{\odot}$  and the largest IC 1613 at  $M_{\star} \simeq 2 \times 10^8 M_{\odot}$ . While these  $V_{\max} \simeq 40 \text{ km s}^{-1}$  halos are too dense in CDM to host any of the plotted Local Field dwarfs, the same halos in SIDM with  $\sigma/m \geq 0.5 \text{ cm}^2 \text{ g}^{-1}$  are consistent with many of the data points.

los with  $V_{\max} = 40 \text{ km s}^{-1}$ , like Pippin and Merry. In SIDM, unlike in CDM, the predicted density profiles allow this to happen self-consistently. In the right-hand panel of Figure 4 we see that *both* Pegasus and Leo A could be hosted by Merry with  $\sigma/m = 10 \text{ cm}^2 \text{ g}^{-1}$ . In the left-hand panel, both galaxies are consistent with the  $\sigma/m = 50 \text{ cm}^2 \text{ g}^{-1}$  line. Given the obvious halo-to-halo scatter and small number of simulations we have, it is difficult to determine which cross section would be favored, but it is clear that for these halos SIDM predicts central densities much more in line with naive expectations for the stellar mass to halo mass relation at the mass scale of dwarfs.

We extend this analysis to smaller stellar masses in the next subsection, where we also address whether high values of  $\sigma/m$  are forbidden by the dynamics of the Local Group dwarfs.

### 3.4 Are any cross sections too large to accommodate measured densities?

We would like to be able to rule out some range of cross sections on the velocity scale of dwarf galaxies by requiring that dark matter densities at least as high as those observed can be achieved. This is in some sense the inverse of the standard central-density problem: for what SIDM cross sections are galaxies *too dense*?

The densest Local Field galaxies shown in Figure 4 are And XVIII ( $r_{1/2} \simeq 400 \text{ pc}$ ) and And XXVIII ( $r_{1/2} \simeq 300 \text{ pc}$ ) with average densities just under  $0.1 M_{\odot} \text{ pc}^{-3}$ . In practice, the mass uncertainties on these galaxies are so large that it will be difficult to derive stringent constraints. At face value, however, the  $\sigma/m = 10 \text{ cm}^2 \text{ g}^{-1}$  lines do appear to be somewhat under-dense (by a factor of  $\sim 2 - 3$ ) compared to the central data points.

The difficulty in this comparison is that we expect that the core densities of SIDM halos will *increase* with decreasing  $V_{\max}$  (Rocha

et al., 2013). We must account for this possibility in any attempt to rule out a given cross section based on an observed galaxy density.

In order to estimate a  $V_{\max}$  scale that might be reasonable for these galaxies we can turn to abundance matching. These dense dwarfs have  $M_{\star} \simeq 3 - 8 \times 10^5 M_{\odot}$ . According to abundance matching estimates (Garrison-Kimmel et al., 2014a), we expect galaxies in this stellar mass range to reside within  $V_{\max} \simeq 20 - 30 \text{ km s}^{-1}$  halos.

How much denser is a  $V_{\max} = 20 \text{ km s}^{-1}$  halo than a  $V_{\max} = 40 \text{ km s}^{-1}$  halo in SIDM? Figure 5 provides some insight. Plotted are fitted halo core densities (assuming a Burkert 1995 profile),  $\rho_b$ , as a function of  $V_{\max}$  for SIDM simulations with  $\sigma/m = 1 \text{ cm}^2 \text{ g}^{-1}$ . The black squares show halos from the simulations of Rocha et al. (2013) while the colored squares show the two halos discussed in this paper. The dotted line shows a  $\rho_b \propto V_{\max}^{-1}$  scaling (a power law fit to all the plotted points yields  $\rho_b \propto V_{\max}^{-0.9}$ ).

If the same  $V_{\max}^{-1}$  behavior holds for core densities in  $\sigma/m = 10 \text{ cm}^2 \text{ g}^{-1}$  models, then the density of a  $V_{\max} = 20 \text{ km s}^{-1}$  halo would be roughly comparable to the best-fit values for And XVIII and And XXVIII in this case.<sup>2</sup> Such a model then remains viable in the face of current constraints.

Thus it appears difficult to rule out any cross sections based on the observed densities of isolated field dwarfs in the Local Group. The same conclusion holds for Milky Way satellites if one considers Figure 8 of Vogelsberger et al. (2012): SIDM with  $\sigma/m = 10 \text{ cm}^2 \text{ g}^{-1}$  (on the velocity scale of dwarf galaxies) can match the spread of local densities seen for the classical satellites

<sup>2</sup> This assumes a constant SIDM cross section. If the cross section is instead velocity dependent this will change, most likely resulting in a shallower power law fit.

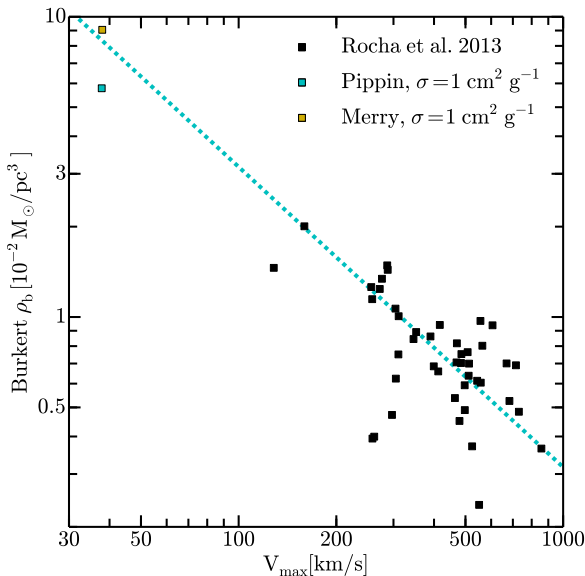


**Figure 5.** Central halo densities of SIDM halos from fitted Burkert (1995) profiles are plotted versus the maximum circular velocities of the halos. Black points are taken from Rocha et al. (2013) and the colored points indicate Merry and Pippin with  $\sigma/m = 1 \text{ cm}^2 \text{ g}^{-1}$ . The dotted line corresponds to a  $1/V_{\text{max}}$  scaling. Though there is significant scatter at fixed mass, smaller halos have higher central densities, helping to naturally explain the “common mass” relation inferred from CDM simulations.

of the Milky Way. A larger simulation suite that includes a range of halo masses and more precise observational mass measurements may eventually allow such a constraint to be derived.

Overall, we emphasize that the puzzling “common mass” relation inferred from collisionless CDM simulations, where luminous galaxies are no more dense, and potentially less dense, than galaxies 1000 times dimmer (as is seen in the Local Group, e.g. Strigari et al., 2008; Boylan-Kolchin et al., 2012; Garrison-Kimmel et al., 2014b), is a natural consequence of SIDM, where halo core densities generally increase with decreasing halo mass.

## 4 CONCLUSIONS

In this work, we have used very high resolution cosmological simulations of  $V_{\text{max}} = 40 \text{ km s}^{-1}$  halos to investigate the effect of SIDM on their density structure. By simulating a range of SIDM cross sections and comparing our simulations to the observed masses of local field dwarfs we have reached the following conclusions:

- SIDM models with  $\sigma/m \simeq 0.5 - 50 \text{ cm}^2 \text{ g}^{-1}$  on the velocity scale of dwarf galaxies ( $v_{\text{rms}} \simeq 40 \text{ km s}^{-1}$ ) alleviate the TBTF problem and produce constant-density core profiles comparable in size to the half-light radii of Local Field dwarfs. It is possible that cross sections even larger than  $50 \text{ cm}^2 \text{ g}^{-1}$  will alleviate the problem without producing catastrophic core collapse.

- The largest ( $\sim 1 \text{ kpc}$ ), lowest density ( $\sim 0.03 M_{\odot} \text{ pc}^{-3}$ ) cores occur for models with  $\sigma/m \simeq 5 - 10 \text{ cm}^2 \text{ g}^{-1}$ . Our single run with  $\sigma/m = 50 \text{ cm}^2 \text{ g}^{-1}$  produces a slightly denser core owing to a mild degree of core collapse, yet it retains a constant-

density profile at small radii and remains significantly less dense than the CDM case.

- SIDM halo core densities increase inversely with halo circular velocity, roughly as  $\rho_{\text{core}} \propto 1/V_{\text{max}}$  (Figure 5). This fact may help explain the unusual trend for less luminous dwarf galaxies to be denser or as dense as galaxies 1000 times brighter (Strigari et al., 2008). However, this behavior also makes it difficult to rule out SIDM models by requiring halos to be at least as dense as the densest known dwarfs (e.g. And XVIII or Draco) since the host  $V_{\text{max}}$  is not well constrained.

A much larger number of simulations, coupled with more precise measurements of dwarf galaxy densities, are required to place tight constraints on  $\sigma/m$  at these velocity scales. Further research, which is currently underway (Vogelsberger et al., 2014; Elbert et al., in preparation; Robles et al., in preparation), is also needed to investigate the effects of baryons on density profiles in an SIDM universe. Overall, however, our results suggest that a wide range of SIDM cross sections remain viable on the velocity scales of dwarf galaxies, and that the range of cross sections that can alleviate TBTF spans at least two orders of magnitude.

## Acknowledgments

The authors thank Manoj Kaplinghat for helpful discussions. Support for this work was provided by NASA through *Hubble Space Telescope* grants HST-GO-12966.003-A and HST-GO-13343.009-A. This work used the Extreme Science and Engineering Discovery Environment (XSEDE), which is supported by National Science Foundation grant number ACI-1053575. We also acknowledge the computational support of the *Greenplanet* cluster at UCI, upon which much of the secondary analysis was performed.

## References

- Amorisco N. C., Zavala J., de Boer T. J. L., 2014, *ApJ*, 782, L39  
 Anderhalden D., Schneider A., Macciò A. V., Diemand J., Bertone G., 2013, *J. Cosmology Astropart. Phys.*, 3, 14  
 Arraki K. S., Klypin A., More S., Trujillo-Gomez S., 2014, *MNRAS*, 438, 1466  
 Balberg S., Shapiro S. L., Inagaki S., 2002, *ApJ*, 568, 475  
 Behroozi P. S., Wechsler R. H., Wu H.-Y., 2013, *ApJ*, 762, 109  
 Boddy K. K., Feng J. L., Kaplinghat M., Shadmi Y., Tait T. M. P., 2014a, arXiv: 1408.6532 [hep-ph]  
 Boddy K. K., Feng J. L., Kaplinghat M., Tait T. M. P., 2014b, *Phys. Rev. D*, 89, 115017  
 Boylan-Kolchin M., Bullock J. S., Kaplinghat M., 2011, *MNRAS*, 415, L40  
 Boylan-Kolchin M., Bullock J. S., Kaplinghat M., 2012, *MNRAS*, 422, 1203  
 Brooks A. M., Zolotov A., 2014, *ApJ*, 786, 87  
 Bryan G. L., Norman M. L., 1998, *ApJ*, 495, 80  
 Buckley M. R., Zavala J., Cyr-Racine F.-Y., Sigurdson K., Vogelsberger M., 2014, *Phys. Rev. D*, 90, 043524  
 Burkert A., 1995, *ApJ*, 447, L25  
 Burkert A., 2000, *ApJ*, 534, L143  
 Cautun M., Frenk C. S., van de Weygaert R., Hellwing W. A., Jones B. J. T., 2014, *MNRAS*, 445, 2049  
 Colín P., Avila-Reese V., Valenzuela O., Firmani C., 2002, *ApJ*, 581, 777  
 Collins M. L. M. et al., 2013, *ApJ*, 768, 172

- Davé R., Spergel D. N., Steinhardt P. J., Wandelt B. D., 2001, *ApJ*, 547, 574
- Del Popolo A., 2012, *MNRAS*, 419, 971
- Del Popolo A., Lima J. A. S., Fabris J. C., Rodrigues D. C., 2014, *J. Cosmology Astropart. Phys.*, 4, 21
- Di Cintio A., Brook C. B., Dutton A. A., Macciò A. V., Stinson G. S., Knebe A., 2014, *MNRAS*, 441, 2986
- Diemand J., Kuhlen M., Madau P., Zemp M., Moore B., Potter D., Stadel J., 2008, *Nature*, 454, 735
- Dubinski J., Carlberg R. G., 1991, *ApJ*, 378, 496
- Epinat B. et al., 2008, *MNRAS*, 388, 500
- Ferrero I., Abadi M. G., Navarro J. F., Sales L. V., Gurovich S., 2012, *MNRAS*, 425, 2817
- Flores R. A., Primack J. R., 1994, *ApJ*, 427, L1
- Fraternali F., Tolstoy E., Irwin M. J., Cole A. A., 2009, *A&A*, 499, 121
- Garrison-Kimmel S., Boylan-Kolchin M., Bullock J. S., Kirby E. N., 2014b, *MNRAS*, 444, 222
- Garrison-Kimmel S., Boylan-Kolchin M., Bullock J. S., Lee K., 2014a, *MNRAS*, 438, 2578
- Garrison-Kimmel S., Horiuchi S., Abazajian K. N., Bullock J. S., Kaplinghat M., 2014c, *MNRAS*, 444, 961
- Garrison-Kimmel S., Rocha M., Boylan-Kolchin M., Bullock J. S., Lally J., 2013, *MNRAS*, 433, 3539
- Gnedin O. Y., Ostriker J. P., 2001, *ApJ*, 561, 61
- Governato F. et al., 2012, *MNRAS*, 422, 1231
- Griest K., 1988, *Phys. Rev. D*, 38, 2357
- Gritschneider M., Lin D. N. C., 2013, *ApJ*, 765, 38
- Hahn O., Abel T., 2011, *MNRAS*, 415, 2101
- Hinshaw G. et al., 2013, *ApJS*, 208, 19
- Hoffman G. L., Salpeter E. E., Farhat B., Roos T., Williams H., Helou G., 1996, *ApJS*, 105, 269
- Horiuchi S., Humphrey P. J., Oñorbe J., Abazajian K. N., Kaplinghat M., Garrison-Kimmel S., 2014, *Phys. Rev. D*, 89, 025017
- Jungman G., Kamionkowski M., Griest K., 1996, *Phys. Rep.*, 267, 195
- Kaplinghat M., Tulin S., Yu H.-B., 2014, *Phys. Rev. D*, 89, 035009
- Katz N., White S. D. M., 1993, *ApJ*, 412, 455
- Kirby E. N., Bullock J. S., Boylan-Kolchin M., Kaplinghat M., Cohen J. G., 2014, *MNRAS*, 439, 1015
- Klypin A., Karachentsev I., Makarov D., Nasonova O., 2014, arXiv: 1405.4523 [astro-ph]
- Koch A., Kleyna J. T., Wilkinson M. I., Grebel E. K., Gilmore G. F., Evans N. W., Wyse R. F. G., Harbeck D. R., 2007, *AJ*, 134, 566
- Kochanek C. S., White M., 2000, *ApJ*, 543, 514
- Koda J., Shapiro P. R., 2011, *MNRAS*, 415, 1125
- Komatsu E. et al., 2011, *ApJS*, 192, 18
- Kuzio de Naray R., McGaugh S. S., de Blok W. J. G., 2008, *ApJ*, 676, 920
- Leaman R. et al., 2012, *ApJ*, 750, 33
- Loeb A., Weiner N., 2011, *Physical Review Letters*, 106, 171302
- Lovell M. R., Frenk C. S., Eke V. R., Jenkins A., Gao L., Theuns T., 2014, *MNRAS*, 439, 300
- Mateo M., Olszewski E. W., Walker M. G., 2008, *ApJ*, 675, 201
- Muñoz R. R. et al., 2005, *ApJ*, 631, L137
- Navarro J. F., Eke V. R., Frenk C. S., 1996, *MNRAS*, 283, L72
- Navarro J. F., Frenk C. S., White S. D. M., 1997, *ApJ*, 490, 493
- Oñorbe J., Garrison-Kimmel S., Maller A. H., Bullock J. S., Rocha M., Hahn O., 2014, *MNRAS*, 437, 1894
- Oh S.-H., de Blok W. J. G., Walter F., Brinks E., Kennicutt, Jr. R. C., 2008, *AJ*, 136, 2761
- Papastergis E., Giovanelli R., Haynes M. P., Shankar F., 2014, arXiv: 1407.4665 [astro-ph]
- Peñarrubia J., Pontzen A., Walker M. G., Koposov S. E., 2012, *ApJ*, 759, L42
- Peter A. H. G., Rocha M., Bullock J. S., Kaplinghat M., 2013, *MNRAS*, 430, 105
- Planck Collaboration et al., 2014, *A&A*, 571, A16
- Polisensky E., Ricotti M., 2014, *MNRAS*, 437, 2922
- Pontzen A., Governato F., 2012, *MNRAS*, 421, 3464
- Power C., Navarro J. F., Jenkins A., Frenk C. S., White S. D. M., Springel V., Stadel J., Quinn T., 2003, *MNRAS*, 338, 14
- Purcell C. W., Zentner A. R., 2012, *J. Cosmology Astropart. Phys.*, 12, 7
- Randall S. W., Markevitch M., Clowe D., Gonzalez A. H., Bradač M., 2008, *ApJ*, 679, 1173
- Reid B. A. et al., 2010, *MNRAS*, 404, 60
- Rocha M., Peter A. H. G., Bullock J. S., Kaplinghat M., Garrison-Kimmel S., Oñorbe J., Moustakas L. A., 2013, *MNRAS*, 430, 81
- Rodríguez-Puebla A., Avila-Reese V., Drory N., 2013, *ApJ*, 773, 172
- Simon J. D., Geha M., 2007, *ApJ*, 670, 313
- Spergel D. N., Steinhardt P. J., 2000, *Physical Review Letters*, 84, 3760
- Springel V., 2005, *MNRAS*, 364, 1105
- Springel V. et al., 2008, *MNRAS*, 391, 1685
- Steigman G., Turner M. S., 1985, *Nuclear Physics B*, 253, 375
- Strigari L. E., Bullock J. S., Kaplinghat M., Simon J. D., Geha M., Willman B., Walker M. G., 2008, *Nature*, 454, 1096
- Strigari L. E., Frenk C. S., White S. D. M., 2014, arXiv: 1406.6079 [astro-ph]
- Tollerud E. J., Boylan-Kolchin M., Bullock J. S., 2014, *MNRAS*, 440, 3511
- Towns J. et al., 2014, *Computing in Science and Engineering*, 99, 1
- Tulin S., Yu H.-B., Zurek K. M., 2013a, *Phys. Rev. D*, 87, 115007
- Tulin S., Yu H.-B., Zurek K. M., 2013b, *Physical Review Letters*, 110, 111301
- Vogelsberger M., Zavala J., 2013, *MNRAS*, 430, 1722
- Vogelsberger M., Zavala J., Loeb A., 2012, *MNRAS*, 423, 3740
- Vogelsberger M., Zavala J., Simpson C., Jenkins A., 2014, *MNRAS*, 444, 3684
- Walker M. G., Mateo M., Olszewski E. W., 2009, *AJ*, 137, 3100
- Walker M. G., Peñarrubia J., 2011, *ApJ*, 742, 20
- Wang J., Frenk C. S., Navarro J. F., Gao L., Sawala T., 2012, *MNRAS*, 424, 2715
- Weiner B. J. et al., 2006, *ApJ*, 653, 1027
- Wolf J., Martinez G. D., Bullock J. S., Kaplinghat M., Geha M., Muñoz R. R., Simon J. D., Avedo F. F., 2010, *MNRAS*, 406, 1220
- Yoshida N., Springel V., White S. D. M., Tormen G., 2000, *ApJ*, 544, L87
- Zavala J., Vogelsberger M., Walker M. G., 2013, *MNRAS*, 431, L20
- Zentner A. R., Bullock J. S., 2002, *Phys. Rev. D*, 66, 043003
- Zolotov A. et al., 2012, *ApJ*, 761, 71

## APPENDIX A: VELOCITY DISPERSION PROFILES

The velocity dispersion profiles of SIDM halos provide insight into the origin and nature of their cored density structures. Figure A1

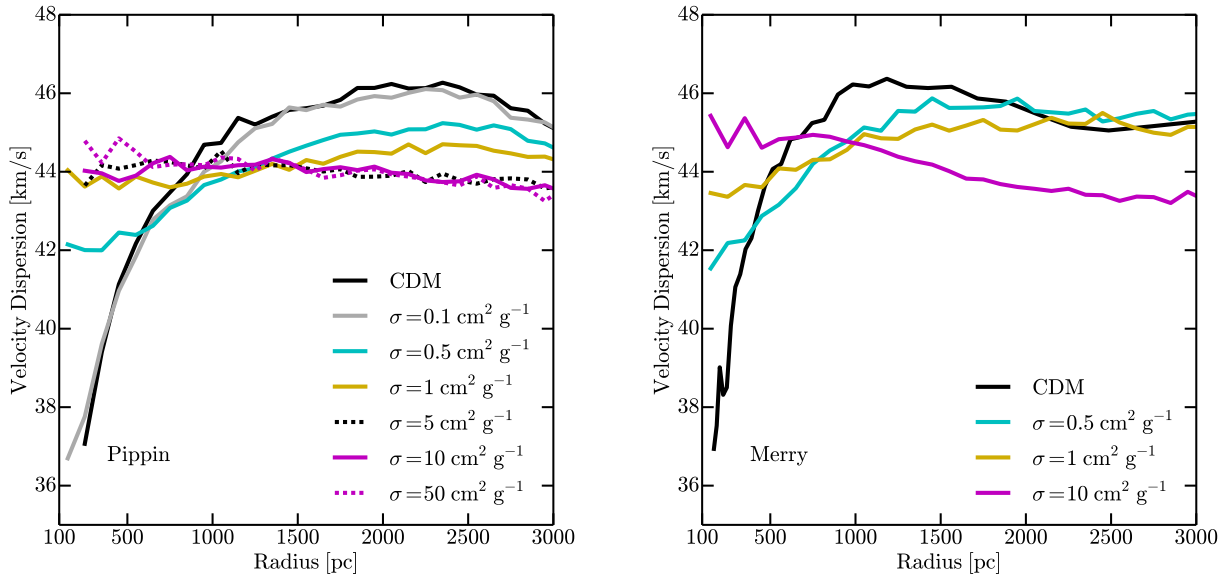


**Figure A1.** Velocity dispersion profiles of Pippin (left) and Merry (right) in collisionless CDM and with a variety of SIDM cross sections (see legend). As the cross section increases to  $\sigma/m = 10 \text{ cm}^2 \text{ g}^{-1}$ , the cores become increasingly hotter and the profiles become more isothermal as kinetic energy is transported to the center of the halo. Very high cross sections  $\sigma/m \geq 10 \text{ cm}^2 \text{ g}^{-1}$  lead to a negative radial gradient, resulting in energy transport from the center of the halo to the outer parts, resulting in mild core collapse and higher central densities, as in the  $50 \text{ cm}^2 \text{ g}^{-1}$  run plotted in Figure 3.

plots the velocity dispersion profiles of our halos both in collisionless CDM and in SIDM, in direct analogy to the density profiles shown in Figure 3. As the SIDM cross section is increased from  $\sigma/m = 0.1 \rightarrow 5 - 10 \text{ cm}^2 \text{ g}^{-1}$ , the cores become steadily hotter and more isothermal as kinetic energy is transported from the outside in (resulting in increasingly lowered central densities relative to the cold cusp that forms in CDM). However, the run with a cross section larger than  $\sigma/m \sim 10 \text{ cm}^2 \text{ g}^{-1}$  begins to display a negative radial gradient – i.e., a core that is hotter than the outer regions. This is precisely the situation where core collapse behavior is expected in SIDM: heat is transferred out of the halo center, resulting in decreased pressure support and ultimately a density enhancement (and further heating). This core collapse behavior is seen explicitly in the left panel of Figure 3, where the Pippin run with  $\sigma/m = 50 \text{ cm}^2 \text{ g}^{-1}$  is much denser than the  $\sigma/m = 5, 10 \text{ cm}^2 \text{ g}^{-1}$  cases.

## APPENDIX B: COMPARISONS TO CLASSICAL MILKY WAY SATELLITES

While Pippin and Merry are isolated dark matter halos, rather than subhalos, it is nonetheless interesting to compare their velocity profiles to the brightest Milky Way dwarf satellites. Figure B1 plots the same circular velocity profiles of Pippin as in Figure 4, but with the data points replaced by measurements of the circular velocities of the bright ( $M_* > 2 \times 10^5 M_\odot$ ) Milky Way satellites used to define TBTF in Boylan-Kolchin et al. (2011, 2012). The points are taken from Wolf et al. (2010), who used data from Muñoz et al. (2005), Koch et al. (2007), Simon & Geha (2007), Mateo et al. (2008), and Walker et al. (2009). As in the field (Figure 4), SIDM runs with  $\sigma/m \geq 0.5 \text{ cm}^2 \text{ g}^{-1}$  alleviate TBTF significantly. Because the simulated halos have not been tidally stripped by a larger host halo,

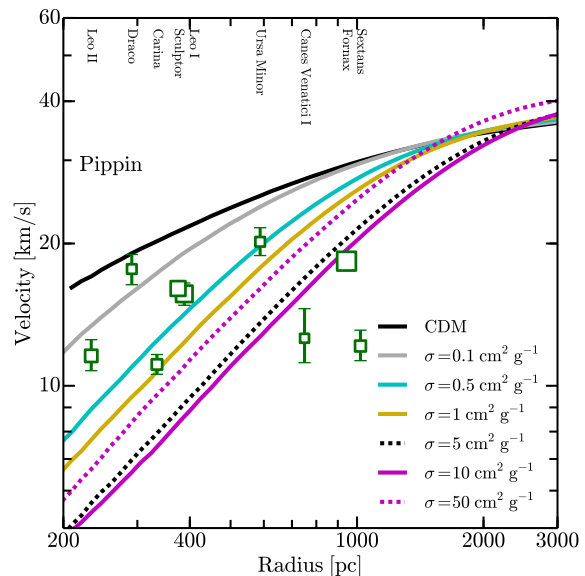


**Figure B1.** Circular velocity profiles of Pippin as in Figure 4, but with constraints on the circular velocities of the bright Milky Way satellites, from Wolf et al. (2010). SIDM simulations with  $\sigma/m \geq 0.5 \text{ cm}^2 \text{ g}^{-1}$  resolve TBTF, as in the field. However, the simulated halos have not undergone the environmental processes typical of subhalos and satellite galaxies; a quantitative comparison is therefore impossible.

however, a quantitative comparison is impossible and we instead present these results for illustrative purposes only.